

## EDGE-BASED SCHWARZ METHODS FOR THE CROUZEIX-RAVIART FINITE VOLUME ELEMENT DISCRETIZATION OF ELLIPTIC PROBLEMS\*

ATLE LONELAND<sup>†</sup>, LESZEK MARCINKOWSKI<sup>‡</sup>, AND TALAL RAHMAN<sup>§</sup>

**Abstract.** In this paper, we present two variants of the additive Schwarz method for a Crouzeix-Raviart finite volume element (CRFVE) discretization of second-order elliptic problems with discontinuous coefficients, where the discontinuities may be across subdomain boundaries. The preconditioner in one variant is symmetric, while in the other variant it is nonsymmetric. The proposed methods are quasi optimal, in the sense that the convergence of the preconditioned GMRES iteration in both cases depend only poly-logarithmically on the ratio of the subdomain size to the mesh size.

**Key words.** domain decomposition, Crouzeix-Raviart element, additive Schwarz method, finite volume element, GMRES

**AMS subject classifications.** 65F10, 65N22, 65N30, 63N55

**1. Introduction.** We introduce and analyze two variants of the additive Schwarz method (ASM) for a Crouzeix-Raviart finite volume element (CRFVE) discretization of second-order elliptic partial differential equations with discontinuous coefficients, where the discontinuities may be across subdomain boundaries. Problems of this type play an important role in scientific computing. Discontinuities or jumps in the coefficient cause the performance of any standard iterative method to deteriorate as the jump increases. The resulting system, which is in general nonsymmetric, is solved using the preconditioned generalized minimal residual (or preconditioned GMRES) method. We consider two variants of the ASM preconditioner, i.e., a symmetric and a nonsymmetric variant. The proposed methods are almost optimal in the sense that the convergence of the GMRES iterations in both cases depends only poly-logarithmically on the ratio of the subdomain size to the mesh size.

The finite volume method divides the computational domain into a set of control volumes whose centroids typically correspond to the nodal points of a finite difference or a finite element discretization. Unlike the finite difference and the finite element method, the solution from a finite volume discretization ensures conservation of certain quantities such as mass, momentum, energy and species. This property is satisfied exactly for each control volume in the domain as well as the whole of the computational domain, connecting the solution to the physics of the system, and, as a consequence, making the method more attractive. There are two types of finite volume methods: one which is based on the finite difference discretization (also known as the finite volume method), and one which is based on the finite element discretization (also known as the finite volume element (FVE) method). In the later case the approximation of the solution is sought in a finite element space, and therefore it can be considered as a Petrov-Galerkin finite element method. Typically, the finite element space is defined on a mesh, called the primal mesh, and the equations are discretized on a mesh which is dual to the primal mesh.

The CRVFE method is a variant of the FVE method, where the solution is sought in the Crouzeix-Raviart (CR) or the P1 nonconforming finite element spaces, as opposed to, say, the

---

\*Received October 25, 2014. Accepted April 30, 2015. Published online on August 21, 2015. Recommended by Olof Widlund. L. Marcinkowski was partially supported by the Polish Scientific Grant 2011/01/B/ST1/01179.

<sup>†</sup>Department of Informatics, University of Bergen, 5020 Bergen, Norway ([Atle.Loneland@ii.uib.no](mailto:Atle.Loneland@ii.uib.no)).

<sup>‡</sup>Faculty of Mathematics, University of Warsaw, Banacha 2, 02-097 Warszawa, Poland  
([Leszek.Marcinkowski@mimuw.edu.pl](mailto:Leszek.Marcinkowski@mimuw.edu.pl)).

<sup>§</sup>Department of Computing, Mathematics and Physics, Bergen University College, Norway  
([Talal.Rahman@hib.no](mailto:Talal.Rahman@hib.no)).

linear conforming or the P1 conforming finite element spaces, which have been commonly used in the earlier works on FVE methods. Although the primal meshes are the same in these two methods, their dual meshes differ significantly since the degrees of freedom of a CR finite element are associated with the edge midpoints and that of a P1 conforming finite element are associated with the vertices. The CRFVE method, which we use in this paper, has been introduced in [6]. For an overview on recent developments of the FVE method, we refer to [15].

Additive Schwarz methods are considered among the most powerful iterative methods for the numerical solution of partial differential equations. There exist quite many works on additive Schwarz methods for symmetric systems arising from the finite element discretizations of second-order elliptic problems; see, e.g., [23, 24] for a complete overview. There are also quite a few works on such methods for the symmetric system resulting from the CR finite element discretization of the problem, some of which can be found in, e.g., [2, 17, 20, 22]. Works on additive Schwarz methods for the nonsymmetric system arising from the FVE discretization of the problem, on the other hand, have been very limited. We refer to [8, 16, 26] for the very few that exist in the literature.

The purpose of this paper is therefore to propose two new algorithms based on the additive Schwarz method for the CRFVE method. The algorithms are based on the edge-based discrete space decomposition, and their analysis is done using the abstract Schwarz framework developed in [18], i.e., an extension of the original abstract Schwarz framework for FE discretization to the FVE discretization. The proposed decomposition of the discrete space is similar to the ones considered in [17] for a nonmatching discretization and in [9] for a discontinuous Galerkin discretization; see also [1, 19, 24] for further references. The proposed methods differ from each other as they use different bilinear forms, i.e., a symmetric and a nonsymmetric bilinear form of the finite element and the finite volume formulations, respectively.

We prove an almost optimal convergence rate for the GMRES iteration applied to the resulting preconditioned systems by showing that one of the two GMRES parameters, which describes the convergence of the GMRES iteration, is bounded above by a constant and the other one, which is the eigenvalue of the symmetric part of the preconditioned system, grows like  $(1 + \log(H/h))^{-2}$ , where  $H$  is the maximal diameter of the subdomains and  $h$  is the mesh size.

The rest of this paper is organized as follows. In Section 2, we present the differential problem and the nonconforming finite volume element discretization. In Section 3 we briefly describe the GMRES method and the corresponding parameters describing its convergence rate. In Section 4 we introduce the two variants of the edge-based Schwarz preconditioner for the CRFVE method and a theorem describing their GMRES convergence rate. In Section 5 we show some numerical results which confirm the theory developed in the previous sections. We also present numerical results to illustrate cases which are not covered by our convergence analysis, namely the cases where the coefficients may have jumps inside subdomains or along subdomain boundaries. Nevertheless the methods seem to work well.

For convenience we use the following notations. For positive constants  $c$  and  $C$ , independent of  $h$  and the coefficients, we define  $u \asymp v$ ,  $x \succeq y$  and  $w \preceq z$  as

$$cu \leq v \leq Cu, \quad x \geq cy \quad \text{and} \quad w \leq Cz,$$

respectively. Here  $u, v, x, y, w$ , and  $z$  are norms of some functions.

## 2. Preliminaries.

**2.1. The model problem.** We consider the following elliptic boundary value problem

$$(2.1) \quad \begin{aligned} -\nabla \cdot (A(x)\nabla u) &= f && \text{in } \Omega, \\ u &= 0 && \text{on } \partial\Omega, \end{aligned}$$

where  $\Omega$  is a bounded convex domain in  $\mathbb{R}^2$  and  $f \in L^2(\Omega)$ .

The corresponding standard variational (weak) formulation is: find  $u \in H_0^1(\Omega)$  such that

$$a(u, v) = \int_{\Omega} f v \, dx \quad \forall v \in H_0^1(\Omega),$$

where

$$a(u, v) = \sum_{k=1}^N \int_{\Omega_k} \nabla u^T A(x) \nabla v \, dx.$$

We partition  $\Omega$  into a set of nonoverlapping subdomains,  $\Omega_i$ , open and connected Lipschitz polytopes such that  $\bar{\Omega} = \bigcup_{i=1}^N \bar{\Omega}_i$ , and assume that they form a coarse triangulation of the domain which is shape-regular with the subdomain size  $H = \max_k H_k$ , where  $H_k = \text{diam } \Omega_k$ . Let  $\Gamma = \bigcup_i \partial\Omega_i \setminus \partial\Omega$  be the global interface.

The coefficient matrix  $A$  restricted to  $\Omega_k$ , i.e.,  $A_k = A|_{\Omega_k}$ , is in  $W^{1,\infty}(\Omega_k)$ , bounded, and symmetric and positive definite, i.e.,

$$(2.2) \quad \exists m_k > 0 \, \forall x \in \Omega_k \, \forall \xi \in \mathbb{R}^2 \quad \xi^T A(x) \xi \geq m_k |\xi|^2$$

$$(2.3) \quad \exists M_k > 0 \, \forall x \in \Omega_k \, \forall \xi, \mu \in \mathbb{R}^2 \quad \mu^T A(x) \xi \leq M_k |\mu| |\xi|.$$

Here  $|\xi| = \sqrt{\xi^T \xi}$ . We can always scale the matrix functions  $A$  in such a way that  $m_k \geq 1$ , for all  $k = 1, \dots, N$ . We also assume that the following bounds hold:  $\|A_k\|_{W^{1,\infty}(\Omega_k)} \leq C_1$ , and  $M_k \leq C_2 m_k$ , with  $C_1, C_2$  positive constants, i.e., we assume that the coefficient matrix locally is smooth, isotropic, and not too much varying.

**2.2. Basic notations.** Throughout this paper we will use the following notation for the Sobolev spaces. The space of functions with generalized derivatives of orders up to  $s$  in the space  $L^2(G)$  is denoted by  $H^s(G)$ . The norm on the space  $H^s(G)$  is defined as

$$\|u\|_{H^s(G)} = \left( \int_G \sum_{|\alpha| \leq s} |D^\alpha u|^2 \, dx \right)^{1/2}.$$

The space of functions with bounded weak derivatives of orders up to  $s$  is denoted by  $W^{s,\infty}(G)$  with the corresponding norm defined as

$$\|u\|_{W^{s,\infty}(G)} = \max_{0 \leq |\alpha| \leq s} \|D^\alpha u\|_{L^\infty(G)}.$$

The subspace of  $H^1(\Omega)$  with functions vanishing on the boundary  $\partial\Omega$  in the sense of traces is denoted by  $H_0^1(\Omega)$ .

We assume that there exists a sequence of quasiuniform triangulations  $\mathcal{T}_h = \mathcal{T}_h(\Omega) = \{\tau\}$  of  $\Omega$ , such that any element  $\tau$  of  $\mathcal{T}_h$  is contained in only one subdomain, consequently, any

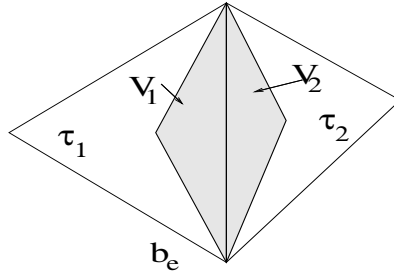


FIG. 2.1. Control volume  $b_e$  (shaded region) associated with the edge  $e$  which is a common edge of the two elements  $\tau_1$  and  $\tau_2$  of the triangulation  $\mathcal{T}_h$ .

subdomain  $\Omega_k$  inherits a sequence of local triangulations,  $\mathcal{T}_h(\Omega_k) = \{\tau\}_{\tau \subset \Omega_k, \tau \in \mathcal{T}_h}$ . With this triangulation  $\mathcal{T}_h(\Omega)$ , we define the broken  $H^1(\Omega)$  norm and seminorm respectively as

$$\|v\|_{H_h^1(\Omega)} = \left( \sum_{\tau \in \mathcal{T}_h(\Omega)} \|v\|_{H^1(\tau)}^2 \right)^{1/2} \quad \text{and} \quad |v|_{H_h^1(\Omega)} = \left( \sum_{\tau \in \mathcal{T}_h(\Omega)} |v|_{H^1(\tau)}^2 \right)^{1/2}.$$

Let  $h = \max_{\tau \in \mathcal{T}_h(\Omega)} \text{diam}(\tau)$  be the mesh size parameter associated with the triangulation. We introduce the following sets of Crouzeix-Raviart (CR) nodal points or nodes:  $\Omega_h, \partial\Omega_h, \Omega_{h,k}, \partial\Omega_{h,k}, \Gamma_h,$  and  $\Gamma_{kl,h}$  are the sets of edge midpoints of  $\mathcal{T}_h$ , which belong to  $\Omega, \partial\Omega, \Omega_k, \partial\Omega_k, \Gamma,$  and  $\Gamma_{kl}$ , respectively. Here  $\Gamma_{kl}$  is an interface, which is an open edge shared by the two subdomains  $\Omega_k$  and  $\Omega_l$ . Note that  $\Gamma_h = \bigcup_{\Gamma_{kl} \subset \Gamma} \Gamma_{kl,h}$ .

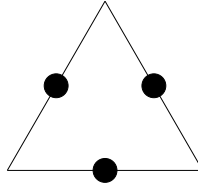


FIG. 2.2. The degrees of freedom of the Crouzeix-Raviart finite element.

Now we define a triangulation  $\mathcal{T}_h^*$  which is dual to  $\mathcal{T}_h$ . Let  $e$  be an edge common to  $\tau_1$  and  $\tau_2$ , two elements of the triangulation  $\mathcal{T}_h$ , such that  $e = \partial\tau_1 \cap \partial\tau_2$ . For  $k = 1, 2$ , let  $V_k \subset \tau_k$  be the triangle obtained by connecting the two endpoints of  $e$  to the centroid (barycenter) of  $\tau_k$ . The control volume associated with the edge  $e$  is then  $b_e = V_1 \cup e \cup V_2$ ; cf. Figure 2.1. If  $e$  is an edge on the boundary  $\partial\Omega$ , then the control volume  $b_e$  associated with the edge will be the triangle obtained by connecting the two endpoints of  $e$  with the centroid of the  $\tau$  for which  $e \subset \partial\tau$ . Then  $\mathcal{T}_h^* = \{b_e\}_{e \in E_h}$  forms the dual triangulation with  $E_h$  being the set of all edges of elements in the triangulation  $\mathcal{T}_h$ .

**2.3. Discrete problem.** In this section we present the Crouzeix-Raviart finite element (CRFE) and the Crouzeix-Raviart finite volume element (CRFVE) discretizations of a model second-order elliptic problem with discontinuous coefficients across subdomain boundaries. The corresponding discrete spaces are defined as follows,

$$\begin{aligned} V_h &:= \{v \in L^2(\Omega) : v|_{\tau} \in P_1, \quad \tau \in \mathcal{T}_h, \quad v \text{ is continuous in } \Omega_h, \\ &\quad v(m) = 0, \quad m \in \partial\Omega_h\}, \\ V_h^* &:= \{v \in L^2(\Omega) : v|_{b_e} \in P_0, \quad b_e \in \mathcal{T}_h^*, \quad v(m) = 0 \quad m \in \partial\Omega_h\}. \end{aligned}$$

$V_h$  is the classical Crouzeix-Raviart finite element space, whose degrees of freedom are associated with the edge midpoints; cf. Figure 2.2 for an illustration.  $V_h^*$  is the space of functions that are piecewise constant over the control volumes and zero on the boundary of the domain. Both spaces are contained in  $L^2(\Omega)$ .

Let  $\{\phi_m\}_{m \in \Omega_h}$  be the standard CR nodal basis of  $V_h$  and  $\{\psi_m\}_{m \in \Omega_h}$  be the standard basis of  $V_h^*$  consisting of characteristic functions of the control volumes.

We also introduce the two interpolation operators,  $I_h$  and  $I_h^*$  defined as follows: for any function  $u$  with properly defined and unique values at the edge midpoints  $m \in \Omega_h$ , we have

$$I_h(u) = \sum_{m \in \Omega_h} u(m)\phi_m, \quad I_h^*(u) = \sum_{m \in \Omega_h} u(m)\psi_m.$$

Note that  $I_h I_h^* u = u$  for any  $u \in V_h$  and  $I_h^* I_h u = u$  for any  $u \in V_h^*$ . Let the nonconforming finite volume element bilinear form  $a_h : V_h \times V_h^* \rightarrow \mathbb{R}$  be defined as:

$$a^{CRFV}(u, v) = - \sum_{e \in E_h^{in}} v(m_e) \int_{\partial b_e} A(s) \nabla u \cdot \mathbf{n} \, ds,$$

where  $\mathbf{n}$  is the outward unit normal vector to  $\partial b_e$ ,  $m_e$  is the midpoint of the edge  $e$ , and  $E_h^{in}$  is the set of all interior edges, i.e., those which are not on  $\partial\Omega$ .

Then our discrete CRFVE problem is to find  $u^{FV} \in V_h$  such that

$$(2.4) \quad a^{FV}(u^{FV}, v) = f(I_h^* v) \quad \forall v \in V_h,$$

for  $a^{FV}(u, v) := a^{CRFV}(u, I_h^* v)$ . In general this problem is nonsymmetric unless the coefficient matrix is a piecewise constant matrix over the elements of  $\mathcal{T}_h(\Omega)$ . One can prove that there exists an  $h_0 > 0$  such that for all  $h \leq h_0$  the form  $a^{FV}(u, v)$  is positive definite over  $V_h$ ; cf. [18]. Thus, this problem has a unique solution. Some error estimates are also proven; cf. [16] for the case of discontinuous coefficients and [6] for the case of smooth coefficients.

The corresponding symmetric nonconforming finite element problem is defined as: find  $u^{FE} \in V_h$  such that

$$a_h(u^{FE}, v) = (f, v), \quad v \in V_h,$$

where the bilinear form  $a_h(\cdot, \cdot)$  is defined as

$$a_h(u, v) = \sum_{\tau \in \mathcal{T}_h} \int_{\tau} \nabla u^T A(x) \nabla v \, dx, \quad u, v \in V_h.$$

The bilinear form  $a_h(\cdot, \cdot)$  also induces the so called energy norm which is defined as  $\|\cdot\|_a = \sqrt{a_h(\cdot, \cdot)}$ .

The next lemma is crucial for the analysis of our method. It relates the two bilinear forms. The proof can be found in [16].

LEMMA 2.1. *For the bilinear forms  $a_h(u, v)$  and  $a^{FV}(u, v)$ , there exists an  $h_0 > 0$  such that, if  $h \leq h_0$ , then the following holds:*

$$|a_h(u, v) - a^{FV}(u, v)| \leq h \|u\|_a \|v\|_a, \quad \forall u, v \in V_h.$$

**3. The GMRES method.** The linear system of equations which arises from problem (2.4) is in general nonsymmetric. We may solve such a system using a preconditioned GMRES method; cf. Saad and Schultz [21], and Eistenstat, Elman and Schultz [11]. This method has proven to be quite powerful for a large class of nonsymmetric problems. The method, which was originally developed in the Euclidean norm, cf. [11], extends easily to the energy norm; cf. [4, 5].

In this paper, we use the GMRES method to solve the linear system of equations

$$Tu = g,$$

where  $T$  is a non-singular nonsymmetric operator,  $g \in V_h$  is the right-hand side, and  $u \in V_h$  is the solution vector.

The main idea of the GMRES method is to solve a least-squares problem at each iteration. At step  $m$  we approximate the exact solution  $u^* = T^{-1}g$  by a vector  $u_m \in \mathcal{K}_m$  which minimizes the norm of the residual, where  $\mathcal{K}_m$  is the  $m$ -th Krylov subspace defined as

$$\mathcal{K}_m = \text{span} \{r_0, Tr_0, \dots, T^{m-1}r_0\},$$

$r_0 = g - Tu_0$  the initial residual, and  $u_0$  the initial guess. Equivalently if  $z_m$  solves

$$\min_{z \in \mathcal{K}_m} \|g - T(u_0 + z)\|_a,$$

then the  $m$ -th iterate becomes  $u_m = u_0 + z_m$ .

The convergence rate of the GMRES method is usually expressed in terms of the following two parameters,

$$(3.1) \quad c_p = \inf_{u \neq 0} \frac{a(Tu, u)}{\|u\|_a^2} \quad \text{and} \quad C_p = \sup_{u \neq 0} \frac{\|Tu\|_a}{\|u\|_a},$$

where  $c_p$  corresponds to the smallest eigenvalue of the symmetric part of  $T$  and  $C_p$  corresponds to the largest eigenvalue of  $T^tT$ . The convergence is given in the following theorem.

**THEOREM 3.1** (Eisenstat-Elman-Schultz). *If  $c_p > 0$ , then the GMRES method converges, and after  $m$  steps the norm of the residual is bounded by*

$$\|r_m\|_a \leq \left(1 - \frac{c_p^2}{C_p^2}\right)^{m/2} \|r_0\|_a,$$

where  $r_m = g - Tu_m$  is the  $m$ -th residual.

The two parameters describing the convergence rate of the GMRES method for the proposed preconditioners will be estimated in Theorem 4.4.

**4. The additive Schwarz method.** In this section, we introduce the two variants of the additive Schwarz method for the discrete problem (2.4), the symmetric and the nonsymmetric variant, and provide estimates of their convergence rate following the abstract framework of [18]. For each subdomain  $\Omega_k$ , define the restriction of  $V_h$  onto  $\Omega_k$ , and the corresponding subspace with zero boundary conditions as

$$V_h(\Omega_k) := \{v|_{\Omega_k} : v \in V_h\}$$

and

$$V_{h,0}(\Omega_k) := \{v \in V_h(\Omega_k) : v(m) = 0 \text{ for } m \in \partial\Omega_{h,k}\} \subset V_h(\Omega_k),$$

respectively. These local spaces are equipped with the bilinear form

$$a_k(u, v) = \sum_{\tau \in \mathcal{T}_h(\Omega_k)} \int_{\tau} \nabla u^T A(x) \nabla v \, dx.$$

Now let  $\mathcal{P}_k : V_h(\Omega_k) \rightarrow V_{h,0}(\Omega_k)$  be the orthogonal projection of a function  $u \in V_h$  onto  $V_{h,0}(\Omega_k)$ , such that

$$a_k(\mathcal{P}_k u, v) = a_k(u, v) \quad \forall v \in V_{h,0}(\Omega_k),$$

and let  $\mathcal{H}_k u = u - \mathcal{P}_k u$  be the discrete harmonic counterpart of  $u$ , that is

$$(4.1) \quad \begin{aligned} a_k(\mathcal{H}_k u, v) &= 0 & \forall v \in V_{h,0}(\Omega_k), \\ \mathcal{H}_k u(m) &= u(m) & m \in \partial\Omega_{h,k}. \end{aligned}$$

A function  $u \in V_h(\Omega_k)$  is locally discrete harmonic if  $\mathcal{H}_k u = u$ . We say that  $u \in V_h$  is discrete harmonic if it is locally discrete harmonic in all subdomains, that is, if

$$u|_{\Omega_k} = \mathcal{H}_k u|_{\Omega_k} \quad \text{for } k = 1, \dots, N.$$

For any function  $u \in V_h$ , this gives a decomposition of  $u$  into locally discrete harmonic parts and local projections, i.e.,  $u = \mathcal{H}u + \mathcal{P}u$ , where  $\mathcal{H}u = (\mathcal{H}_1 u, \dots, \mathcal{H}_N u)$  and  $\mathcal{P}u = (\mathcal{P}_1 u, \dots, \mathcal{P}_N u)$ .

Discrete harmonic functions satisfy the minimal energy property, that is,  $u = \mathcal{H}_k u \in V_h(\Omega_k)$  has the minimal energy among all functions which are equal to  $u$  on  $\partial\Omega_{h,k}$ , that is,

$$a_k(u, u) = \min \{ a_k(v, v) : v(p) = u(p) \quad \forall p \in \partial\Omega_{h,k} \}.$$

By (4.1) the values of a discrete harmonic functions at the interior CR nodal points of the subdomains are completely determined by the values on  $\partial\Omega_{h,k}$ .

**4.1. Decomposition of  $V_h$ .** To define our additive Schwarz method we first need to introduce a decomposition of the space  $V_h$  into subspaces equipped with local bilinear forms. The space  $V_h$  is decomposed into the following subspaces: a coarse space  $V_0$ , local edge spaces  $V_{kl}$  for  $\Gamma_{kl} \subset \Gamma$ , and local subdomain spaces  $V_k$  for  $k = 1, \dots, N$ .

We start by defining special edge functions that we will use to build our coarse space.

**DEFINITION 4.1.** *Let  $\Gamma_{kl} \subset \Gamma$  be the edge common to  $\Omega_k$  and  $\Omega_l$ , and let  $\theta_{kl} \in V_h$  be the corresponding discrete harmonic function defined by its values at the CR nodal points of  $\Gamma_h$  as follows,*

- $\theta_{kl}(p) = 1 \quad p \in \Gamma_{kl,h}$ ,
- $\theta_{kl}(p) = 0 \quad p \in \Gamma_h \setminus \Gamma_{kl,h}$ .

*The support of the edge function  $\theta_{kl}$  is  $\Omega_k \cup \Gamma_{kl} \cup \Omega_l$ ; cf. Figure 4.1.*

The coarse space is then defined as the span of all edge functions  $\theta_{kl}$  associated with  $\Gamma_{kl} \subset \Gamma$ , that is,

$$V_0 = \text{span}\{\theta_{kl}\}_{\Gamma_{kl} \subset \Gamma} \subset V_h.$$

The local edge space  $V_{kl}$  associated with the edge  $\Gamma_{kl}$ , where  $\Gamma_{kl} \subset \Gamma$ , is defined as the space of discrete harmonic functions determined by their values at the CR nodal points of  $\Gamma_{kl,h}$  and may be nonzero only at the nodal points of  $\Omega_{k,h} \cup \Gamma_{kl,h} \cup \Omega_{l,h}$ .

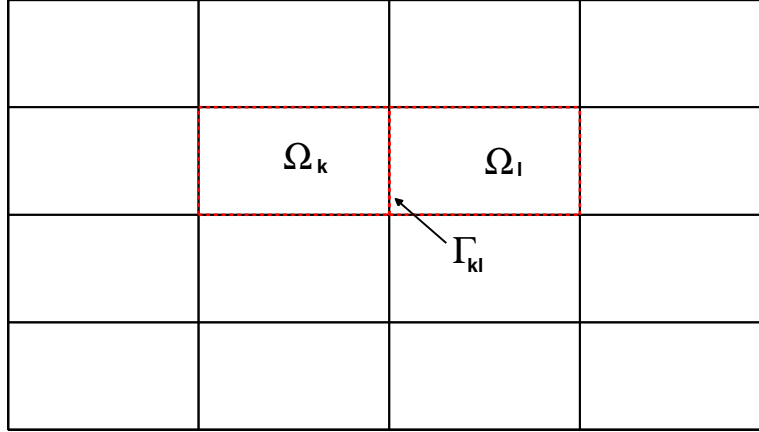


FIG. 4.1. Support of an edge function  $\theta_{kl}$  corresponding to the interface  $\Gamma_{kl}$ .

The local subdomain space  $V_k$  associated with the subdomain  $\Omega_k$ , where  $k = 1, \dots, N$ , is the space  $V_{h,0}(\Omega_k)$  extended by zero to the remaining subdomains.

We have the following decomposition of our discrete space  $V_h$ ,

$$V_h = V_0 + \sum_{\Gamma_{kl} \subset \Gamma} V_{kl} + \sum_{k=1}^N V_k.$$

We now introduce the following symmetric projection-like operators based on the symmetric bilinear form  $a_h(\cdot, \cdot)$ . For  $i = 0, \dots, N$ , the projection-like operators  $T_i^{sym}: V_h \rightarrow V_i$  associated with the coarse space and the local subdomain spaces are defined as

$$a_h(T_i^{sym} u, v) = a^{FV}(u, v) \quad \forall v \in V_i,$$

while the projection-like operators  $T_{kl}^{sym}: V_h \rightarrow V_{kl}$ , associated with the edge  $\Gamma_{kl}$  for  $\Gamma_{kl} \subset \Gamma$ , are defined as

$$a_h(T_{kl}^{sym} u, v) = a^{FV}(u, v) \quad \forall v \in V_{kl}.$$

We note that computing  $T_i^{sym} u$  and  $T_{kl}^{sym} u$  corresponds to solving local symmetric CRFE Dirichlet problems, and the solutions are unique.

The nonsymmetric projection-like operators based on the nonsymmetric bilinear form  $a^{FV}(\cdot, \cdot)$  are defined analogously. For  $i = 0, \dots, N$ , the corresponding projection-like operators  $T_i^{nsym}: V_h \rightarrow V_i$  associated with the coarse space and the local subdomain spaces are defined as

$$a^{FV}(T_i^{nsym} u, v) = a^{FV}(u, v) \quad \forall v \in V_i,$$

while the projection-like operators  $T_{kl}^{nsym}: V_h \rightarrow V_{kl}$ , associated with the edge  $\Gamma_{kl}$  for  $\Gamma_{kl} \subset \Gamma$ , are defined as

$$a^{FV}(T_{kl}^{nsym} u, v) = a^{FV}(u, v) \quad \forall v \in V_{kl}.$$

Again, computing  $T_i^{nsym} u$  and  $T_{kl}^{nsym} u$  corresponds to solving local nonsymmetric CRVFE Dirichlet problems, the solutions of which are unique.

We now introduce the additive Schwarz operator  $T^{type}$  as

$$T^{type} := \sum_{\Gamma_{kl} \subset \Gamma} T_{kl}^{type} + \sum_{k=0}^N T_k^{type},$$

where the super-index  $type$  denotes either  $sym$  or  $nsym$ , referring to the operator as symmetric or nonsymmetric, respectively. We can now replace the original problem (2.4) with the equivalent preconditioned system of equations

$$(4.2) \quad T^{type} u^{FV} = g^{type}.$$

where  $g^{type}$  is defined as

$$g^{type} = g_0^{type} + \sum_{\Gamma_{kl} \subset \Gamma} g_{kl}^{type} + \sum_{k=1}^N g_k^{type}$$

with  $g_0^{type} = T_0^{type} u^{FV}$ , and  $g_{kl}^{type} = T_{kl}^{type} u^{FV}$ ,  $g_k^{type} = T_k^{type} u^{FV}$ . Note that  $g_i^{type}$  can be computed without knowing the solution  $u^{FV}$ ; cf., e.g., [23, 24].

**4.2. Analysis.** Before we state our main theorem on the convergence of our proposed method, we mention two main lemmas which are needed in our analysis in order to estimate the parameters describing the GMRES convergence. For their proofs, we refer to [17].

LEMMA 4.2. *Let  $\Gamma_{kl} \subset \Gamma$  be an edge, and  $\theta_{kl}$  the corresponding edge function from Definition 4.1. Then for any  $u \in V_h$  we have*

$$(4.3) \quad \begin{aligned} |\theta_{kl}|_{H_h^1(\Omega_k)}^2 &\preceq \left(1 + \log\left(\frac{H_k}{h}\right)\right), \\ |u_{kl}|_{H_h^1(\Omega_k)}^2 &\preceq \left(1 + \log\left(\frac{H_k}{h}\right)\right)^2 (H_k^{-2} \|u\|_{L^2(\Omega_k)}^2 + |u|_{H_h^1(\Omega_k)}^2), \end{aligned}$$

where  $u_{kl}$  is a function taking the same values as  $\theta_{kl}u$  at the CR nodal points on  $\partial\Omega_k$ .

LEMMA 4.3. *For any  $u = \sum_{\Gamma_{kl}} u_{kl} \theta_{kl} \in V_0$  the following holds*

$$a_k(u, u) \preceq M_k \left(1 + \log\left(\frac{H_k}{h}\right)\right) \left(\sum_{\Gamma_{kl} \neq \Gamma_{ik}} (u_{kl} - u_{ik})^2\right),$$

where  $M_k$  is from (2.3),  $u_{kl} = u|_{\Gamma_{kl}}$ , and the sum is taken over all pairs of edges  $\Gamma_{kl}$ ,  $\Gamma_{ik} \subset \partial\Omega_k$ .

We are now ready to state the main theorem for the convergence rate of our additive Schwarz method applied to nonsymmetric problem (2.4).

THEOREM 4.4. *There exists an  $h_0 > 0$  such that for all  $h < h_0$ ,  $k = 1, 2$ , and  $u \in V_h$ , we have*

$$\begin{aligned} \|T^{type} u\|_a &\preceq \|u\|_a, \\ a_h(T^{type} u, u) &\succeq \left(1 + \log\left(\frac{H}{h}\right)\right)^{-2} a_h(u, u), \end{aligned}$$

*Proof.* Following the framework of [18] we need to prove three key assumptions; cf. Appendix A.

ASSUMPTION 1'. *There exists an  $h_0 > 0$  such that, if  $h \leq h_0$ , for all  $u, v \in V_h$ , then the following holds*

$$|a_h(u, v) - a^{FV}(u, v)| \leq h \|u\|_a \|v\|_a,$$

This is exactly Lemma 2.1.

ASSUMPTION 2'. *For all  $u \in V_h$  there exists a constant  $C > 0$  such that there is a representation  $u = u_0 + \sum_{i=1}^N u_i + \sum_{kl} u_{kl}$ , with  $u_0 \in V_0, u_i \in V_i, u_{kl} \in V_{kl}$ , such that*

$$a_h(u_0, u_0) + \sum_{i=1}^N a_h(u_i, u_i) + \sum_{kl} a_h(u_{kl}, u_{kl}) \leq C \left(1 + \log \left(\frac{H}{h}\right)\right)^2 a_h(u, u).$$

This assumption is the same as what is known as the ‘‘stable decomposition’’ or the ‘‘Assumption 1’’ in the abstract Schwarz framework; cf. [23, 24]. To verify the assumption we first need to define a decomposition of the function  $u \in V_h$ . Following the lines of the proof of Lemma 6.1 in [17], we start by letting  $u_0 \in V_0$  be defined as  $u_0 = \sum_{kl} \bar{u}_{kl} \theta_{kl}$ , where  $\bar{u}_{kl}$  is the average of  $u$  over  $\Gamma_{kl}$ .

Next, let  $w = u - u_0$ , and for each  $k = 1, \dots, N$ , define  $u_k \in V_k$  as  $u_k = \mathcal{P}_k w$  on  $\Omega_k$  and zero outside the subdomain  $\Omega_k$ . Note that  $\mathcal{P}_k w = \mathcal{P}_k u$  since  $u_0$  is discrete harmonic and also  $w - \sum_{k=1}^N u_k$  is discrete harmonic in each subdomain. Now define  $u_{kl} \in V_{kl}$  at the CR nodal points of  $\Gamma_{kl,h}$  as

$$u_{kl}(p) = \theta_{kl}(p)w(p), \quad \forall p \in \Gamma_{kl,h}.$$

Clearly  $u = u_0 + \sum_{i=1}^N u_i + \sum_{kl} u_{kl}$ .

To validate Assumption 2' we start by estimating  $a_h(u_0, u_0)$ . From Lemma 4.3 and the Schwarz inequality we have

$$\begin{aligned} a_h(u_0, u_0) &\leq \sum_{k=1}^N M_k \left(1 + \log \left(\frac{H_k}{h}\right)\right) \sum_{\Gamma_{kl}, \Gamma_{ik} \subset \partial\Omega_k} |\bar{u}_{kl} - \bar{u}_{ik}|^2 \\ &\leq \sum_{k=1}^N M_k \left(1 + \log \left(\frac{H_k}{h}\right)\right) \frac{1}{H} \sum_{\Gamma_{kj} \subset \partial\Omega_k} \|u - \bar{u}_{kl}\|_{L^2(\Gamma_{kj})}^2, \end{aligned}$$

where  $\Gamma_{kl}$  is an arbitrary edge of  $\Omega_k$ . Applying standard trace theorem arguments, Poincaré's inequality for nonconforming elements, cf. [2, 3, 22], and (2.2)–(2.3), we get

$$\begin{aligned} (4.4) \quad a_h(u_0, u_0) &\leq \sum_{k=1}^N \frac{M_k}{m_k} \left(1 + \log \left(\frac{H_k}{h}\right)\right) a_k(u, u) \\ &\leq \left(1 + \log \left(\frac{H_k}{h}\right)\right) a_h(u, u). \end{aligned}$$

Next, we estimate the term  $a_h(u_k, u_k)$  for  $u_k \in V_k$ , for  $k = 1, \dots, N$ . Using the fact that  $\mathcal{P}_k$  is an orthogonal projection with respect to the local bilinear form  $a_k(\cdot, \cdot)$  and Lemma 4.3, we have

$$\begin{aligned} \sum_{k=1}^N a_h(u_k, u_k) &= \sum_{k=1}^N a_k(\mathcal{P}_k w, \mathcal{P}_k w) \leq a_h(w, w), \\ &\leq a_h(u_0, u_0) + a_h(u, u). \end{aligned}$$

From (4.4) it then follows that

$$(4.5) \quad \sum_{k=1}^N a_h(u_k, u_k) \preceq \left(1 + \log\left(\frac{H_k}{h}\right)\right) a_h(u, u).$$

Finally, we estimate the term  $a_k(u_{kl}, u_{kl})$  for  $u_{kl} \in V_{kl}$ , for  $\Gamma_{kl} \subset \Gamma$ . Using (4.3) in Lemma 4.2, the Poincaré inequality for nonconforming finite elements, and (2.2)–(2.3), we get

$$\begin{aligned} a_k(u_{kl}, u_{kl}) &\leq M_k |u_{kl}|_{H_h^1(\Omega_k)}^2, \\ &\preceq M_k \left(1 + \log\left(\frac{H_k}{h}\right)\right)^2 \left(\frac{1}{H_k^2} \|u - \bar{u}_{kl}\|_{L^2(\Omega_k)}^2 + |u - \bar{u}_{kl}|_{H_h^1(\Omega_k)}^2\right) \\ &\preceq M_k \left(1 + \log\left(\frac{H_k}{h}\right)\right)^2 |u|_{H_h^1(\Omega_k)}^2 \preceq \frac{M_k}{m_k} \left(1 + \log\left(\frac{H_k}{h}\right)\right)^2 a_k(u, u) \\ &\preceq \left(1 + \log\left(\frac{H_k}{h}\right)\right)^2 a_k(u, u) \end{aligned}$$

Summing the above estimate over all edges  $\Gamma_{kl} \subset \Gamma$ , we get

$$(4.6) \quad \begin{aligned} \sum_{kl} a_k(u_{kl}, u_{kl}) &\preceq \sum_{k=1}^N \left(1 + \log\left(\frac{H_k}{h}\right)\right)^2 a_k(u, u), \\ &\leq \left(1 + \log\left(\frac{H}{h}\right)\right)^2 a_h(u, u). \end{aligned}$$

Summing (4.4), (4.5) and (4.6) completes the proof.

For Assumption 3, which is the same as what is known as the “strengthened Cauchy-Schwarz inequalities” in the standard abstract Schwarz framework, cf. [23, 24], it follows immediately from the standard coloring argument that the constants from these inequalities are bounded. The proof of the theorem now follows from the abstract framework.  $\square$

**REMARK 4.5.** In our analysis, we have used several technical tools, e.g., the trace theorem and the Poincaré inequality for the CR finite element, Lemmas 4.3 and 4.2. They are all based on the assumption that the subdomains are regular polygons. Therefore, we cannot straightforwardly apply our analysis to the case of subdomains with less regular boundaries. However, we think that using the results from [10, 14, 25], it will be possible to extend our analysis to the case of less regular subdomains.

**5. Numerical results.** In this section, we present some numerical results for the proposed method. All experiments are done for the model problem (2.1) on the unit square domain  $\Omega = [0, 1]^2$ , using the symmetric and the nonsymmetric variant of the method, i.e., for  $type = \{sym, nsym\}$ . For the numerical experiments under consideration, the coefficient  $A$  will be strongly varying with possible discontinuities across subdomain boundaries. For completeness, in the last two numerical experiments, we allow the coefficient  $A$  to also have discontinuities inside the subdomains and along the subdomain boundaries. The right-hand side for all the numerical experiments under consideration is chosen as  $f = 1$ . We have used direct solvers for the coarse and the subspace solves. We note that if the same exact solver (based on for instance the LU factorization) is used for both the symmetric and the nonsymmetric case, the two variants of the preconditioner will have the same computational cost if the number of iterations are the same. In the case when one uses a direct solver (based on the Cholesky factorization) exploiting the symmetric property of the local systems,

the symmetric variant of the preconditioner will be slightly more computationally effective than the nonsymmetric variant. This effect is very marginal for the numerical experiments considered here.

The numerical solution is found by using the generalized minimal residual (GMRES) method accelerated with either the symmetric or the nonsymmetric preconditioners. We run the method until the  $l_2$  norm of the initial residual is reduced by a factor of  $10^6$ , that is, until  $\|r_i\|_2/\|r_0\|_2 \leq 10^{-6}$ . For all the numerical experiments under consideration we report the number of iterations and the estimate for the smallest eigenvalue of the symmetric part of the preconditioned operator  $T$ , i.e., the smallest eigenvalue of  $\frac{1}{2}(T^t + T)$ , with respect to the  $a$ -inner product. This is the parameter  $c_p$  in (3.1), which describes the convergence rate of the GMRES method; cf. Theorem 3.1. In our case, it is also the main parameter describing the GMRES convergence rate since both our analysis and numerical experiments have shown that the other parameter  $C_p$  in (3.1) is a constant independent of the underlying mesh parameters and the coefficient  $A$ .

**5.1. Regular subdomains.**

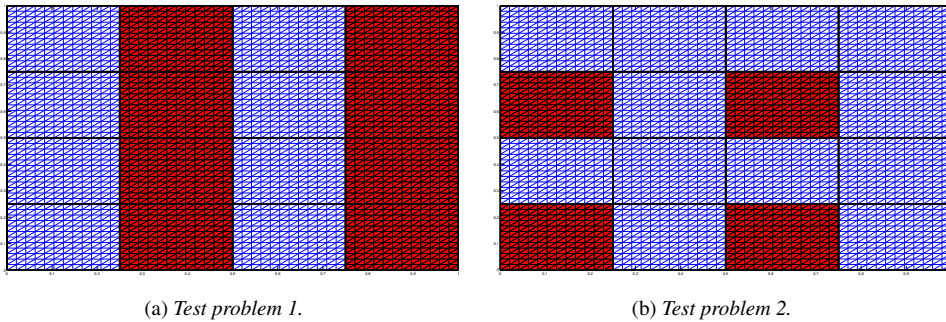


FIG. 5.1. Test problems 1 and 2. The red (shaded) regions are where  $\alpha_1$  equals  $\hat{\alpha}_1$ . The fine mesh consists of  $48 \times 48$  rectangular blocks, while the coarse mesh consists of  $4 \times 4$  rectangular subdomains.

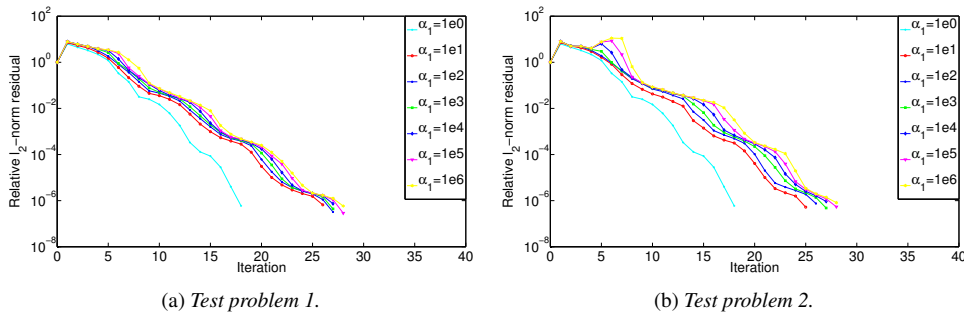


FIG. 5.2. Relative residual norms versus GMRES iteration (minimizing the  $a$ -norm) for different values of  $\hat{\alpha}_1$ . These values, as shown in the figure legends, are listed against  $\alpha_1$ .

We first consider two test problems with the fine mesh size  $h = 1/48$  and the coarse mesh size  $H = 1/4$  and discontinuities across subdomain boundaries. The coefficient  $A$  is equal to  $\alpha_1(2 + \sin(100\pi x) \sin(100\pi y))$ . The parameter  $\alpha_1$  is piecewise constant and equal to  $\hat{\alpha}_1$  in the regions (subdomains) marked with red (shaded) and 1 elsewhere; cf. Figure 5.1. In other words,  $\alpha_1$  describes where the coefficient  $A$  has jumps. The preconditioner we employ

TABLE 5.1

*Number of GMRES iterations until convergence for the solution of (2.4), with different values of  $\hat{\alpha}_1$  describing the coefficient  $A = \alpha_1(2 + \sin(100\pi x) \sin(100\pi y))$  in the red (shaded) regions; cf. Figure 5.1.*

$\hat{\alpha}_1$	Problem 1:	Problem 2:
$10^0$	18 (2.15e-1)	18 (2.15e-1)
$10^1$	25 (2.14e-1)	26 (2.09e-1)
$10^2$	26 (2.14e-1)	27 (2.07e-1)
$10^3$	27 (2.14e-1)	27 (2.06e-1)
$10^4$	27 (2.14e-1)	27 (2.06e-1)
$10^5$	27 (2.14e-1)	28 (2.06e-1)
$10^6$	28 (2.14e-1)	28 (2.06e-1)

for these experiments is the symmetric variant, i.e., for  $type = sym$  in (4.2). The number of iterations is reported in Table 5.1 with estimates of the smallest eigenvalue of the symmetric part of the preconditioned system (4.2) in parentheses next to the iteration count. In Figure 5.2 we have plotted the relative residuals for these problems, measured in the  $l_2$  norm.

We see from the number of iterations and the eigenvalue estimates in Table 5.1 that they reflect well the theoretical results developed in Section 4.2. We do not see any dependency on the contrast in the coefficient  $A$ , where the jumps are across subdomain boundaries.

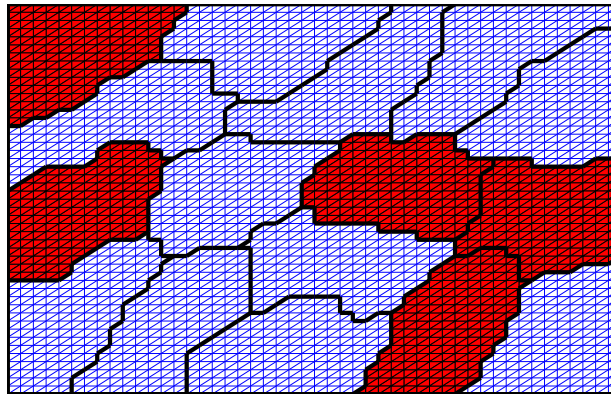


FIG. 5.3. *Test problem 3. The red (shaded) regions are where  $\alpha_1$  equals  $\hat{\alpha}_1$  and 1 elsewhere. The fine mesh consists of  $48 \times 48$  rectangular blocks, while the coarse mesh consists of 16 irregular subdomains.*

**5.2. Irregular subdomains.** Here we show a test case to illustrate that the method can be applied to problems with less regular subdomains such as the ones stemming from a mesh partitioning software, like METIS [13] or SCOTCH [7]. For this example we have used METIS for the partitioning of  $\Omega$  into subdomains. The coefficient distributions are as shown in Figure 5.3, and the number of iterations and estimates of the smallest eigenvalues are given in Table 5.2.

We see from the results that, although the iteration numbers are slightly higher than in the regular case, both variants of the method seem robust with respect to the jumps in the coefficient across subdomain boundaries.

TABLE 5.2

Test problem 3. Number of GMRES iterations until convergence for different values of  $\hat{\alpha}_1$  in the coefficient  $A = \alpha_1(2 + \sin(100\pi x) \sin(100\pi y))$ ; cf. Figure 5.3.

$\hat{\alpha}_1$	Symmetric variant	Non-symmetric variant
	# iter.	# iter.
$10^0$	28 (1.93e-1)	28 (1.92e-1)
$10^1$	32 (1.60e-1)	31 (1.60e-1)
$10^2$	33 (1.37e-1)	32 (1.37e-1)
$10^3$	34 (1.34e-1)	33 (1.35e-1)
$10^4$	35 (1.34e-1)	33 (1.35e-1)
$10^5$	35 (1.34e-1)	35 (1.34e-1)
$10^6$	36 (1.34e-1)	35 (1.34e-1)

**5.3. Scalability.** In the following experiments we show the asymptotic dependence of the parameter  $c_p$  on the mesh parameters  $H$  and  $h$ . For the purpose, we use two test cases where the coefficient  $A$  is equal to  $2 + \sin(10\pi x) \sin(10\pi y)$  and  $2 + \sin(100\pi x) \sin(100\pi y)$ , respectively. The number of iterations and the estimates of the smallest eigenvalue are reported in Tables 5.3 and 5.4 for the symmetric variant of the preconditioner. For comparison, we also report in Table 5.5 the asymptotic dependency on the mesh parameters  $H$  and  $h$  for the nonsymmetric variant of the preconditioner. The distribution of  $A$  here is the same as for the problem considered in Table 5.4.

By looking at the number of iterations and the eigenvalue estimates in Tables 5.3–5.4, we see that they change very slowly with respect to the change in  $h$  and  $H$ . This suggest a logarithmic bound that is in line with our theory which states that the parameters describing the convergence rate of the GMRES method depend poly-logarithmically on the mesh ratio  $\frac{H}{h}$ . Also, by comparing Table 5.4 and 5.5, we see that the difference in the behavior of the symmetric and the nonsymmetric preconditioner is negligible. The two preconditioners perform almost identically for the problem at hand, both with respect to the iteration number and the behavior of the smallest eigenvalue.

TABLE 5.3

Iteration number and estimate of the smallest eigenvalue for the symmetric preconditioner for increasing values of  $h$  and  $H$  with  $A = 2 + \sin(10\pi x) \sin(10\pi y)$ .

$h/H$	1/4	1/8	1/16	1/32	1/64	1/128
1/8	13 (5.31e-1)					
1/16	16 (3.47e-1)	17 (4.86e-1)				
1/32	17 (2.26e-1)	20 (3.44e-1)	17(4.85e-1)			
1/64	19 (1.62e-1)	24 (2.51e-1)	20 (3.46e-1)	17 (4.85e-1)		
1/128	21 (1.24e-1)	28 (1.86e-1)	24 (2.60e-1)	20 (3.45e-1)	16 (4.85e-1)	
1/256	24 (9.84e-2)	32 (1.41e-1)	29 (1.90e-1)	23 (2.63e-1)	19 (3.47e-1)	16 (4.85e-1)

**5.4. Jumps inside subdomains and along subdomain boundaries.** Here we consider two test problems for the symmetric and the nonsymmetric variant of the preconditioner where the coefficients have large and possibly different jumps inside the subdomains and along the subdomain boundaries. The motivation for these experiments is to show that even though our convergence analysis does not cover these cases, both the symmetric and the nonsymmetric variants of the method work well for the two examples given. For both experiments, the

TABLE 5.4

*Iteration number and estimate of the smallest eigenvalue for the symmetric preconditioner for increasing values of  $h$  and  $H$  with  $A = 2 + \sin(100\pi x) \sin(100\pi y)$ .*

$h/H$	1/4	1/8	1/16	1/32	1/64	1/128
1/8	12 (5.32e-1)					
1/16	14 (3.64e-1)	17 (4.85e-1)				
1/32	16 (2.64e-1)	19 (3.45e-1)	18 (4.73e-1)			
1/64	19 (1.87e-1)	22 (2.60e-1)	21 (3.36e-1)	18 (4.73e-1)		
1/128	22 (1.39e-1)	28(1.82e-1)	25 (2.52e-1)	22 (3.37e-1)	20 (4.65e-1)	
1/256	24 (1.07e-1)	35(1.26e-1)	34 (1.66e-1)	25 (2.56e-1)	25 (3.26e-1)	19 (4.78e-1)

TABLE 5.5

*Iteration number and estimate of the smallest eigenvalue for the nonsymmetric preconditioner for increasing values of  $h$  and  $H$  with  $A = 2 + \sin(100\pi x) \sin(100\pi y)$ .*

$h/H$	1/4	1/8	1/16	1/32	1/64	1/128
1/8	11 (5.35e-1)					
1/16	13 (3.67e-1)	15 (4.98e-1)				
1/32	15 (2.62e-1)	19 (3.48e-1)	17 (4.71e-1)			
1/64	18 (1.88e-1)	22 (2.53e-1)	21 (3.31e-1)	17 (4.81e-1)		
1/128	21 (1.39e-1)	29 (1.75e-1)	26 (2.45e-1)	21 (3.41e-1)	19 (4.73e-1)	
1/256	24 (1.07e-1)	36 (1.24e-1)	33 (1.61e-1)	26 (2.58e-1)	24 (3.24e-1)	18 (4.83e-1)

coefficient is given as  $A = \alpha_1 (2 + \sin(10\pi x) \sin(10\pi y))$  where  $\alpha_1$  is shown in Figures 5.4–5.5. The parameter  $\alpha_1$  is piecewise constant and equal to  $\hat{\alpha}_1$  in the regions marked with colors (shaded) and 1 elsewhere.

For the first of the two problems, we allow  $\hat{\alpha}_1$  to have three different values inside the subdomains: these are regions marked with the colors red (squares), blue (horizontal rectangles), and black (vertical rectangles); cf. Figure 5.4. In Table 5.6, we show the number of iterations and estimates of the smallest eigenvalue in parentheses next to the iteration count.

The numerical results show that the two preconditioners work well for this case. This is not so surprising. It is well known that domain decomposition methods with coarse spaces based on functions which are discrete harmonic extension of some prescribed boundary values are robust for problems with jumps inside the subdomains; cf. [12] or [16] for the case of average extension. This has also been confirmed with extensive numerical testing for the two methods considered in this paper.

In the last numerical experiments, we allow  $A$  to have large jumps along the subdomain boundaries in addition to having jumps inside the subdomains. We see from the Table 5.7 that even for this coefficient distribution, the two preconditioners behave well in this case. Here, the situation is less clear. The exact relation between the contrast in the coefficient and the convergence estimate for the case where the coefficient has jumps along the subdomain boundaries for this method, is unknown. The numerical testing carried out so far has shown that, as long as the inclusions are away from the vertices/corner points of the subdomains or the inclusions do not form a channel touching two or more of the interfaces between subdomains, the two variants of the preconditioners work very well.

The extension of our convergence analysis to multiscale problems will be the topic of further research.

**Acknowledgments.** The authors would like to thank Professor Petter Bjørstad and Professor Maksymilian Dryja for their valuable comments and discussions.

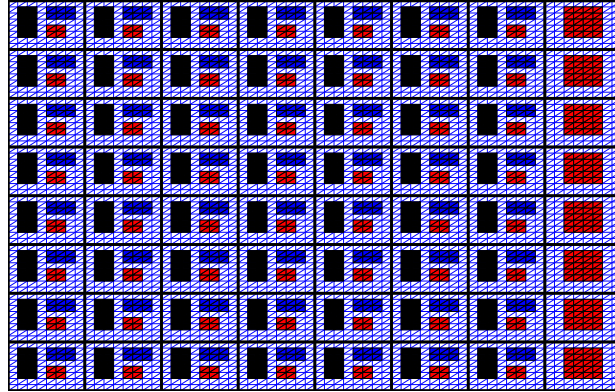


FIG. 5.4. Test problem 4. The colored (shaded) regions, including the red (squared) regions, the blue (horizontal rectangular) regions, and the black (vertical rectangular) regions, are regions where  $\alpha_1$  equals  $\hat{\alpha}_1$  and 1 elsewhere.  $\hat{\alpha}_1$  takes different values in different colored (geometrical) regions. The fine mesh consists of  $64 \times 64$  rectangular blocks, while the coarse mesh consists of  $8 \times 8$  rectangular subdomains.

TABLE 5.6

Test problem 4. Number of GMRES iterations until convergence for different values of  $\hat{\alpha}_1$  in the coefficient  $A = \alpha_1(2 + \sin(10\pi x) \sin(10\pi y))$ ; cf. Figure 5.4.

$\hat{\alpha}_1$			Symmetric variant	Non-symmetric variant
Red:	Blue:	Black:	‡ iter.	‡ iter.
$10^0$	$10^{-2}$	$10^{-3}$	32 (1.63e-1)	32 (1.62e-1)
$10^1$	$10^{-1}$	$10^{-2}$	31 (1.83e-1)	31 (1.82e-1)
$10^2$	$10^0$	$10^{-1}$	27 (2.27e-1)	27 (2.25e-1)
$10^3$	$10^1$	$10^0$	24 (3.00e-1)	24 (2.98e-1)
$10^4$	$10^2$	$10^1$	22 (3.32e-1)	22 (3.31e-1)
$10^5$	$10^3$	$10^2$	22 (3.36e-1)	22 (3.35e-1)
$10^6$	$10^4$	$10^3$	22 (3.37e-1)	22 (3.36e-1)

**Appendix A. The abstract framework for FVE discretization; cf. [18].** Consider a family of finite dimensional finite element subspaces  $V_h$  with mesh parameter  $h$ , an inner product  $a(\cdot, \cdot)$  on  $V_h$ , and a family of discrete problems. Find  $u_h \in V_h$  such that

$$(A.1) \quad a^{FV}(u_h, v) = f(v) \quad \forall v \in V_h,$$

where  $a^{FV}(u, v)$  is a nonsymmetric finite volume bilinear form.

Continuing, we decompose  $V_h$  into subspaces as follows,

$$V_h(\Omega) = V_0 + \sum_{i=1}^N V_i,$$

where  $V_i \subset V_h$  for  $i = 0, \dots, N$ .

For each subspace  $V_i$ , we introduce a projection-like operators  $T_i : V_h(\Omega) \rightarrow V_i$ , such that

$$(A.2) \quad a(T_i u, v) = a^{FV}(u, v) \quad \forall v \in V_i,$$

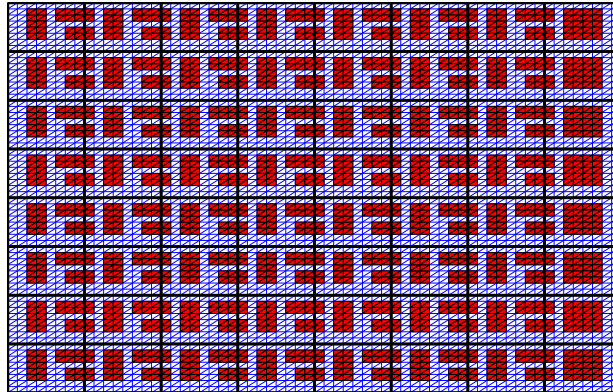


FIG. 5.5. Test problem 5. The red (shaded) regions are where  $\alpha_1$  equals  $\hat{\alpha}_1$  and 1 elsewhere. The fine mesh consists of  $64 \times 64$  rectangular blocks, while the coarse mesh consists of  $8 \times 8$  rectangular subdomains.

TABLE 5.7

Test problem 5. Number of GMRES iterations until convergence for different values of  $\hat{\alpha}_1$  in the coefficient  $A = \alpha_1(2 + \sin(10\pi x) \sin(10\pi y))$ ; cf. Figure 5.5.

$\hat{\alpha}_1$	Symmetric variant	Non-symmetric variant
	# iter.	# iter.
$10^0$	24 (2.51e-1)	24 (2.50e-1)
$10^1$	22 (3.33e-1)	22 (3.32e-1)
$10^2$	22 (3.46e-1)	22 (3.45e-1)
$10^3$	22 (3.47e-1)	22 (3.46e-1)
$10^4$	22 (3.47e-1)	22 (3.46e-1)
$10^5$	22 (3.47e-1)	22 (3.46e-1)
$10^6$	22 (3.47e-1)	22 (3.46e-1)

and the symmetric additive operator

$$T := T_0 + T_1 + \cdots + T_N.$$

We replace the original problem (A.1) by the following operator equation

$$Tu_h = g,$$

where  $g = \sum_{i=0}^N g_i$  and  $g_i = T_i u_h$ , which can be computed without knowing the solution  $u$ .

The nonsymmetric version of the operator  $T$  can be constructed completely analogously by replacing the form  $a(\cdot, \cdot)$  by  $a^{FV}(\cdot, \cdot)$  in (A.2).

ASSUMPTION 1. There exist positive constants  $C_E, h_0$  such that, if  $h \leq h_0$ , then for all  $u, v \in V_h$  the following holds

$$|a(u, v) - a^{FV}(u, I_h^* v)| \leq C_E h \|u\|_a \|v\|_a.$$

ASSUMPTION 2. There exists a positive constant  $C_0$  such that for all  $u \in V_h$  there exists a representation  $u = \sum_{i=0}^N u_i$ ,  $u_i \in V_i$ , such that

$$\sum_{i=0}^N a(u_i, u_i) \leq C_0^2 a(u, u).$$

ASSUMPTION 3. Let  $0 \leq \mathcal{E}_{ij} \leq 1$  be the minimal values that satisfy

$$a(u_i, u_j) \leq \mathcal{E}_{ij} \|u_i\|_a \|u_j\|_a, \quad \forall u_i \in V_i, \forall u_j \in V_j \quad i, j = 1, \dots, N.$$

We let  $\rho(\mathcal{E})$  be the spectral radius of the symmetric matrix  $\mathcal{E} = \{\mathcal{E}_{ij}\}_{i,j=1}^N$ .

Assumption 1 yields that there exists  $0 < h_1 \leq h_0$  such that the bilinear form  $a^{FV}(\cdot, \cdot)$  is  $V_h$ -elliptic and  $V_h$ -bounded for  $h \leq h_1$ , i.e., there exist positive constants  $\alpha, M$  such that

$$\begin{aligned} a^{FV}(u, u) &\geq \alpha \|u\|_a^2 && \forall u \in V_h, \\ |a^{FV}(u, v)| &\leq M \|u\|_a \|v\|_a && \forall u, v \in V_h. \end{aligned}$$

With these assumptions satisfied, the estimates of the parameters describing the GMRES convergence are given in the following theorem.

THEOREM A.1. *There exists an  $h_1 \leq h_0$  such that, if  $h \leq h_1$ , then*

$$\begin{aligned} a(Tu, Tu) &\leq \beta_2^2 a(u, u), \\ a(Tu, u) &\geq \beta_1 a(u, u), \end{aligned}$$

where  $\beta_2 = (2M(1 + \rho(\mathcal{E})))$  and  $\beta_1 = (\alpha^2 C_0^{-2} - \beta_2 C_E h)$ .

#### REFERENCES

- [1] J. H. BRAMBLE, J. E. PASCIAK, AND A. H. SCHATZ, *The construction of preconditioners for elliptic problems by substructuring. I*, Math. Comp., 47 (1986), pp. 103–134.
- [2] S. C. BRENNER, *Two-level additive Schwarz preconditioners for nonconforming finite element methods*, Math. Comp., 65 (1996), pp. 897–921.
- [3] ———, *Poincaré-Friedrichs inequalities for piecewise  $H^1$  functions*, SIAM J. Numer. Anal., 41 (2003), pp. 306–324.
- [4] X.-C. CAI, *Some Domain Decomposition Algorithms for Nonselfadjoint Elliptic and Parabolic Partial Differential Equations*, Ph.D. Thesis, Courant Institute, New York University, New York, 1989.
- [5] X.-C. CAI AND O. B. WIDLUND, *Domain decomposition algorithms for indefinite elliptic problems*, SIAM J. Sci. Statist. Comput., 13 (1992), pp. 243–258.
- [6] P. CHATZIPANTELIDIS, *A finite volume method based on the Crouzeix-Raviart element for elliptic PDE's in two dimensions*, Numer. Math., 82 (1999), pp. 409–432.
- [7] C. CHEVALIER AND F. PELLEGRINI, *PT-Scotch: a tool for efficient parallel graph ordering*, Parallel Comput., 34 (2008), pp. 318–331.
- [8] S. H. CHOU AND J. HUANG, *A domain decomposition algorithm for general covolume methods for elliptic problems*, J. Numer. Math., 11 (2003), pp. 179–194.
- [9] E. T. CHUNG, H. H. KIM, AND O. B. WIDLUND, *Two-level overlapping Schwarz algorithms for a staggered discontinuous Galerkin method*, SIAM J. Numer. Anal., 51 (2013), pp. 47–67.
- [10] C. R. DOHRMANN, A. KLAWONN, AND O. B. WIDLUND, *Domain decomposition for less regular subdomains: overlapping Schwarz in two dimensions*, SIAM J. Numer. Anal., 46 (2008), pp. 2153–2168.
- [11] S. C. EISENSTAT, H. C. ELMAN, AND M. H. SCHULTZ, *Variational iterative methods for nonsymmetric systems of linear equations*, SIAM J. Numer. Anal., 20 (1983), pp. 345–357.
- [12] I. G. GRAHAM, P. O. LECHNER, AND R. SCHEICHL, *Domain decomposition for multiscale PDEs*, Numer. Math., 106 (2007), pp. 589–626.
- [13] G. KARYPIS AND V. KUMAR, *A fast and high quality multilevel scheme for partitioning irregular graphs*, SIAM J. Sci. Comput., 20 (1998), pp. 359–392.
- [14] A. KLAWONN, O. RHEINBACH, AND O. B. WIDLUND, *An analysis of a FETI-DP algorithm on irregular subdomains in the plane*, SIAM J. Numer. Anal., 46 (2008), pp. 2484–2504.
- [15] Y. LIN, J. LIU, AND M. YANG, *Finite volume element methods: an overview on recent developments*, Int. J. Numer. Anal. Model. Ser. B, 4 (2013), pp. 14–34.
- [16] A. LONELAND, L. MARCINKOWSKI, AND T. RAHMAN, *Additive average Schwarz method for a Crouzeix-Raviart finite volume element discretization of elliptic problems with heterogeneous coefficients*, Preprint on arXiv, 2014. <http://arxiv.org/abs/1405.3494>
- [17] L. MARCINKOWSKI, *Additive Schwarz method for mortar discretization of elliptic problems with  $P_1$  nonconforming finite elements*, BIT, 45 (2005), pp. 375–394.

- [18] L. MARCINKOWSKI, T. RAHMAN, A. LONELAND, AND J. VALDMAN, *Additive schwarz preconditioner for the general finite volume element discretization of symmetric elliptic problems*, Preprint on arXiv, 2014. <http://arxiv.org/abs/1405.0185>
- [19] T. P. A. MATHEW, *Domain Decomposition Methods for the Numerical Solution of Partial Differential Equations*, Springer, Berlin, 2008.
- [20] T. RAHMAN, X. XU, AND R. HOPPE, *Additive Schwarz methods for the Crouzeix-Raviart mortar finite element for elliptic problems with discontinuous coefficients*, Numer. Math., 101 (2005), pp. 551–572.
- [21] Y. SAAD AND M. H. SCHULTZ, *GMRES: a generalized minimal residual algorithm for solving nonsymmetric linear systems*, SIAM J. Sci. Statist. Comput., 7 (1986), pp. 856–869.
- [22] M. SARKIS, *Nonstandard coarse spaces and Schwarz methods for elliptic problems with discontinuous coefficients using non-conforming elements*, Numer. Math., 77 (1997), pp. 383–406.
- [23] B. SMITH, P. BJØRSTAD, AND W. GROPP, *Domain Decomposition: Parallel Multilevel Methods for Elliptic Partial Differential Equations*, Cambridge University Press, Cambridge, 1996.
- [24] A. TOSELLI AND O. WIDLUND, *Domain Decomposition Methods—Algorithms and Theory*, Springer, Berlin, 2005.
- [25] O. B. WIDLUND, *Accommodating irregular subdomains in domain decomposition theory*, in Domain Decomposition Methods in Science and Engineering XVIII, M. Bercovier, M. J. Gander, R. Kornhuber, and O. Widlund, eds., vol. 70 of Lect. Notes Comput. Sci. Eng., Springer, Berlin, 2009, pp. 87–98.
- [26] S. ZHANG, *On domain decomposition algorithms for covolume methods for elliptic problems*, Comput. Methods Appl. Mech. Engrg., 196 (2006), pp. 24–32.